Journal of the European Ceramic Society 22 (2002) 1285–1296

www.elsevier.com/locate/jeurceramsoc

Modelling and numerical simulation of the electrical, mechanical, and thermal coupled behaviour of multilayer capacitors (MLCs)

Klaus Prume[a,*], Klaus Franken[b], Ulrich Böttger[a], Rainer Waser[a], Horst R. Maier[b]

[a]*Institut für Werkstoffe der Elektrotechnik, Lehrstuhl II, RWTH Aachen, Aachen, Germany*
[b]*Institut für Keramische Komponenten im Maschinenbau, RWTH Aachen, Aachen, Germany*

Received 21 March 2001; received in revised form 31 July 2001; accepted 15 August 2001

Abstract

The modelling of non-linear coupled material characteristics has been used for finite element simulations of the integral device behaviour and mechanical and electrical stress distributions of ceramic multilayer capacitors. A two-dimensional finite element model of standard X7R-type capacitors of different sizes soldered on a printed circuit board has been developed to calculate residual, joining as well as mechanical and electrical load stresses. This model includes the experimentally measured non-linear bias field dependencies of the electric and piezoelectric characteristics of the $BaTiO_3$ based dielectric material. The validation of the model is demonstrated by calculations of the failure probability of soldered capacitors in a four-point bending test under simultaneous electrical loading. The results allow a description and possible improvement of the short-time reliability under particular load cases.

Keywords: $BaTiO_3$; Capacitors; Electrical properties; Failure analysis; Simulation; Strength

1. Introduction

Multilayer ceramic capacitors (MLCs) according to Fig. 1 with X7R dielectric specified according to the Electronic Industries Association (EIA) standard 198 are the most popular among all ceramic capacitors. They are used mainly for by-pass and coupling or for frequency-discriminating circuits where the temperature and field dependency of capacitance and losses are not of major importance. In contradiction to the very low price of a single MLC the demands for reliability are tremendous. The failure of one capacitor could lead to the malfunction of a complete circuit or component. So, low failure rates of 2.4 failures in time (FIT) = failure rate within 10^9 component hours are typical for these devices. Nevertheless, a better understanding and further reduction of failures is required. For this purpose finite-element (FE) simulations can effectively be used to calculate internal stress distributions and predict the reliability of MLCs. The components are stressed due to the manufacturing process, the high temperature treatment during soldering and electrical and mechanical loading. All of these stresses contribute to the total stress distribution and are dependent on the coupling of the electrical, mechanical, and thermal material characteristics. Hence, the knowledge and measurements of the material characteristics and their dependencies are necessary for the simulations. Based on these data a modelling of the complex metal–ceramic composite structure and the non-linear material behaviour is possible and sources and incidences of internal stresses can be calculated.

2. Characterization of MLCs and experimental

2.1. Dielectric material

The capacitor characteristics and performance are mainly determined by the large and small signal dielectric material behaviour. In general, the material characteristics are dependent on large and small signal changes of the electric field, the mechanical stress, and the temperature. Polycrystalline barium titanate ($BaTiO_3$) is widely used in X7R MLCs as dielectric material. Permittivities of several thousands can be obtained near the phase transitions of this perovskite

* Corresponding author.
E-mail address: prume@aixacct.com (K. Prume).

0955-2219/02/$ - see front matter
PII: S0955-2219(01)00439-3

type material. Typically, highly doped, inhomogeneous ceramics are prepared to reduce the strong temperature dependency of the dielectric constant near the phase transitions.[1] The measurement of the relative capacity change of a type 1210 MLC with 3.3 nF related to the capacity at room temperature in the temperature range from −100 °C to +160 °C for different frequencies is shown in Fig. 2. The indicated box displays the accepted capacity change of ±15% between −55 °C to +125 °C for capacitors which fulfil the X7R specification of the Electronic Industry Association (EIA) standard RS-198-B. The number 1210 depicts the sample size, where the first pair of digits represent the length extension and the second pair of digits represent the width extension in 0.01 inch. Besides the dependency on temperature the permittivity is also strongly related to the applied electrical bias field E_{dc} as shown in Fig. 3. A permittivity drop of up to 90% can be seen with a bias voltage of 10 MV/m at a frequency of 1 kHz and room temperature.

Additionally, the large signal hysteresis loop of the electric polarisation P of a type 1210 MLC with 3.3 nF capacity (Fig. 4) and the mechanical displacement x (Fig. 5) show a non-linear dependency from the electric bias field. These measurements where performed with the TF Analyser 2000 from aixACCT Systems, Aachen. The hysteresis of the polarisation is very small compared to piezoelectric materials like PZT and has a very low remanent value. The stretch reveals a more or less quadratic dependency from the electric field which is comparable to electrostrictive relaxor materials.[2] These curves are important for the modelling and simulation of the device behaviour and mechanical stress distributions under electrical large and small signal loading conditions. The modelling of this behaviour will be described in Section 3.1.

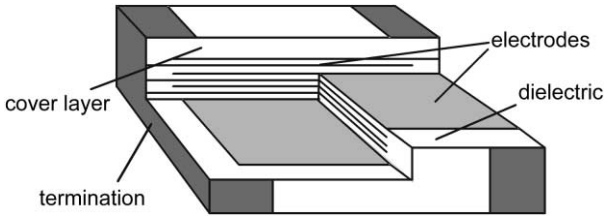

Fig. 1. Schematic design of a multilayer ceramic capacitor.

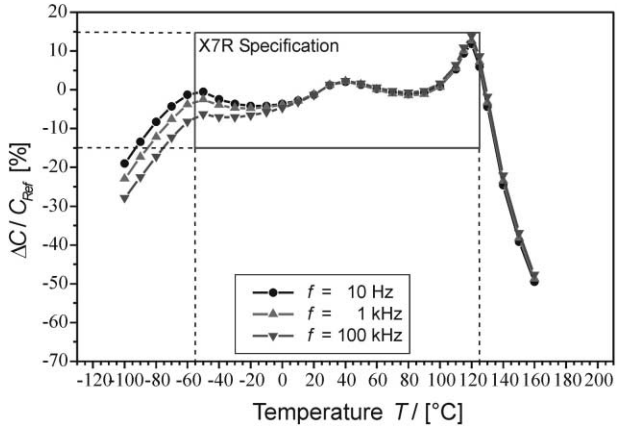

Fig. 2. Temperature dependency of the capacity of a type 1210 MLC with 3.3 nF for different frequencies. The permitted range of capacity deviation of the X7R specification is shown with the sketched box.

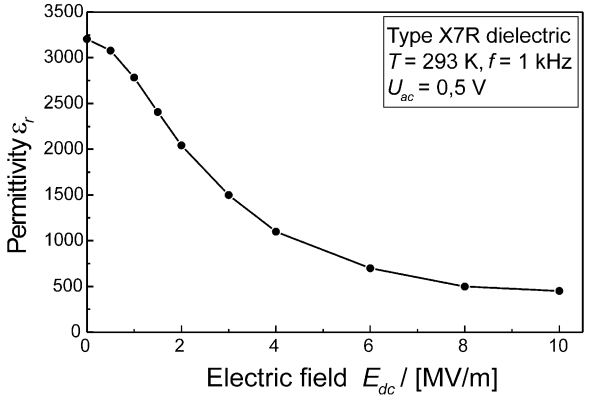

Fig. 3. Dependency of the small signal permittivity from the electric bias field for a X7R type dielectric material.

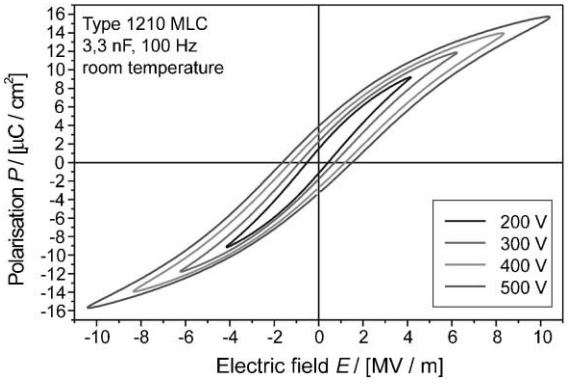

Fig. 4. Hysteresis of the polarisation of a type 1210 MLC with 3.3 nF at 100 Hz with different voltage amplitudes.

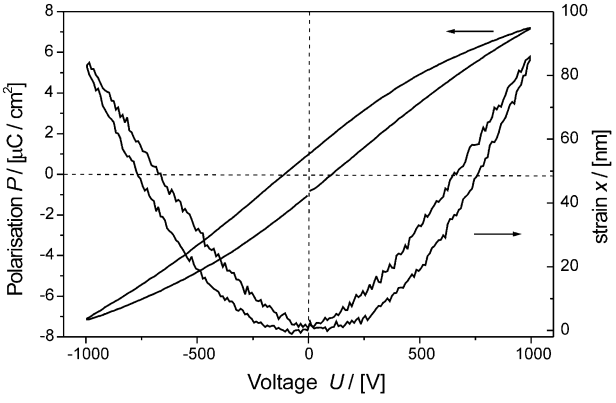

Fig. 5. Overall displacement x and polarisation P vs. large signal voltage for a X7R type, 500 µm thick dielectric.

2.2. Residual stress measurement

Besides the electrical characteristics of the dielectric material knowledge of the mechanical stress distribution of the fabricated device is important. Residual stress measurements were done on different MLCs by the X-ray diffraction using a PW 3070 ψ-diffractometer with the so called Psi-geometry. A linear $\sin^2\psi$ fit has been achieved for plane stress analysis (σ_x instead of σ_{xx}) based on an elastic constant of 91 GPa according to the Voigt model. The first order residual stresses in the x-direction (σ_x) at the surface of the MLCs were measured. The mean stresses at areas of 0.25 mm length and 1.0 mm width were taken along the x-axis between the terminations at steps of 0.2 mm (Fig. 6). Nine single measurements were performed for each measurement point in Fig. 7 which leads to the indicated measurement error. The MLC sizes 1206 (21 nF), 1206 (100 nF), and 1210 (10 nF) were measured. All three sizes show qualitatively the same stress course at different stress levels. There are almost constant compressive stresses in the middle of the component and the stress reaches a minimum a few tenths of mm before the edge of the termination. At the edge of the termination ($x \approx \pm 1.2$ mm) the stress rises with a high gradient up to tensile stress. Typical constant stresses in the middle of the components were between −30 and −60 MPa, the maximum tensile stresses were in the region of 60 MPa. Due to the high stress gradients and the presence of the metallic termination the stress measurements near the termination edges have to looked at with care.

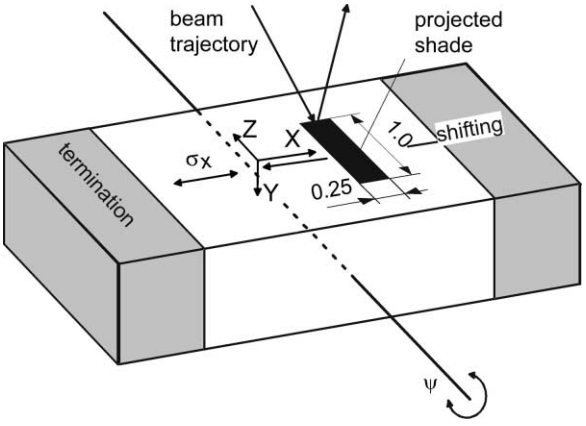

Fig. 6. Principle design of residual stress measurement by X-ray diffraction.

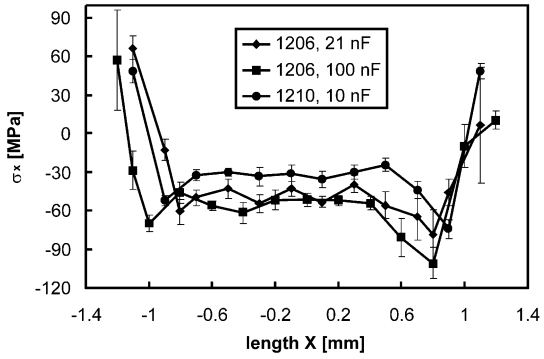

Fig. 7. Residual stresses σ_x along component length of three different MLC sizes.

2.3. Bending test

Bending tests are typical proof tests to check the reliability of soldered MLCs.[3] Tests have been performed with five different sets of MLCs with three different sizes (1206, 1210 with 3.3 nF, and 2220 with 150 nF) and the 1206 size with 1, 56, and 120 nF capacity. Each set contains of about 30 samples. Additional, the test fixture has been extended to apply bias voltages up to 150 V to the samples and to simultaneously measure the MLC capacity for the evaluation of the exact moment of failure. For the bending test the MLCs were soldered to stripes of a printed circuit board (PCB) as shown in Fig. 8. The width of the stripes b was 4 mm for the 1206 and the 1210 sizes, and 7 mm for the 2220 size. The thickness of all PCB stripes was 1.6 mm. The MLCs were dipped in a solder paste (Sn60Pb) and then heated up to 250 °C by hot air to solder them. The bending test was performed by a testing machine (Instron) with a loading rate of 0.5 mm/s, a load span l_{load} of 20 mm, and a support span l_{sup} of 40 mm. During the test the MLC capacity and the load F were measured. Two kinds of fracture were observed. In most cases the MLCs failed totally which was detected by a total loss of the capacity (Fig. 9, left). Sometimes a local fracture was observed which was followed by a partial loss of the capacity (Fig. 9, right). In each case the fracture started at the bottom side of the MLC near the termination edge and was running under an angle into the termination. The fracture load $F_{f,i}$ of each specimen i was defined as the load at the moment of the first significant loss in capacity. The fracture moment $M_{f,i}$ can than be calculated by

$$M_{f,i} = \frac{F_{f,i}}{4}\left(l_{sup} - l_{load}\right). \quad (1)$$

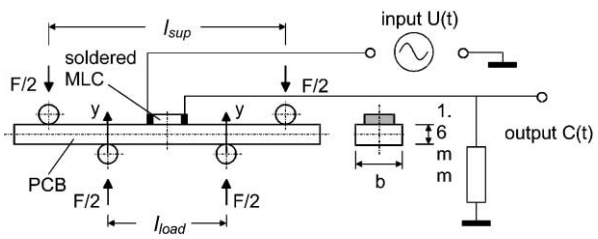

Fig. 8. Principle of the four-point bending facility with electrical loading.

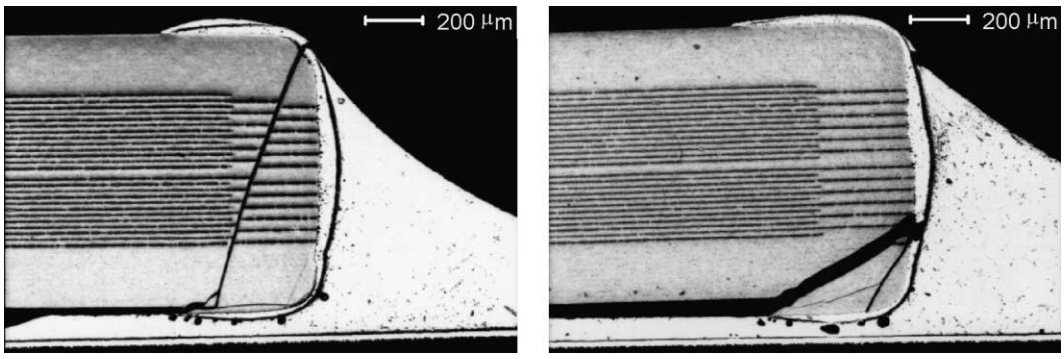

Fig. 9. Typical cracks in the polished cross-sections of soldered MLCs under bending load stress.

To each fracture moment $M_{f,i}$ a failure probability $P_i = i/(n+1)$ can be assigned, where n means the total number of specimens of one measurement series. This estimator is used based on internal comparison, although it is now generally accepted that $P_i = (i-0.5)/n$ yields more accurate estimates for the failure probability. The results for the five different MLC sizes bent without a bias voltage are given in Fig. 10. For one size (1206, 56 nF) the bending test was also performed for the three bias voltages 50, 100 and 150 V to investigate the influence of the electrical loading on the device reliability. These test results are plotted in Fig. 11.

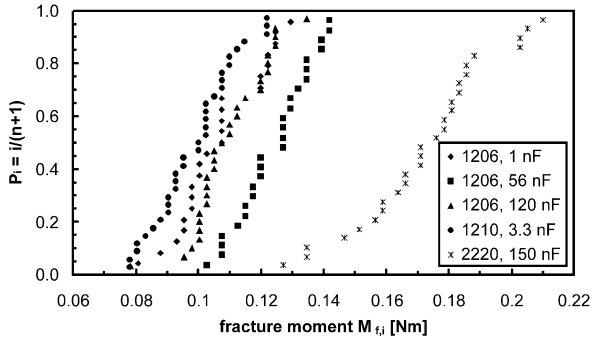

Fig. 10. Measured fracture moments of four-point bending test of five different sets of soldered MLCs (no applied bias voltage).

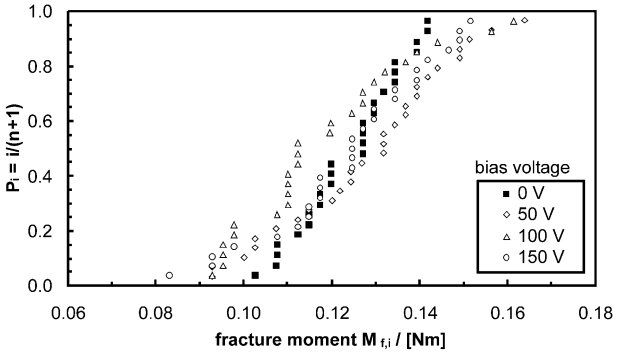

Fig. 11. Measured fracture moments of four-point bending test of a soldered MLC 1206 type (56 nF) for different bias voltages.

3. Modelling

3.1. Electrical and mechanical behaviour

In commercial finite-element programs it is usually not possible to include non-linear electrical material characteristics. Therefore, an individual modelling of the material characteristics presented in Section 2.1 has to be performed. For this reason an ANSYS® macro has been developed to estimate the large signal operating point of the electric displacement $D_0(E_{dc})$ and the mechanical strain $S_0(E_{dc})$ due to an applied electrical bias field E_{dc}. This can be included in the piezoelectric equations with the independent variables σ (mechanical stress) and E (electrical field) which are used by the program:

$$S = S_0(E_{dc}) + c\cdot\sigma + dE \tag{2}$$

$$D = D_0(E_{dc}) + d\cdot\sigma + \varepsilon_r E \tag{3}$$

where c denotes the mechanical stiffness matrix, d the piezoelectric coefficient matrix, and ϵ_r the permittivity matrix. From the polarisation curve in Fig. 4 the non-linear dependency of the electric displacement $D_0(E_{dc})$ is derived, neglecting the hysteresis. This is acceptable

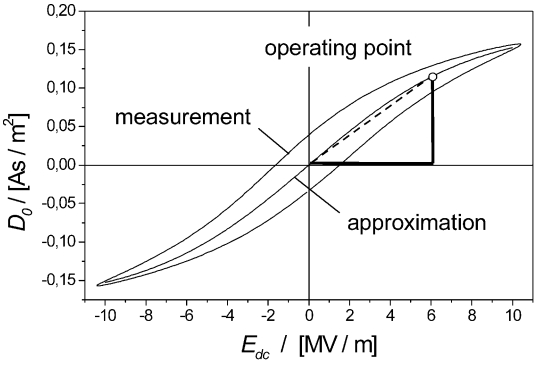

Fig. 12. Bias field dependency of the electric displacement and non-linear approximation curve for the modelling of the large signal operating point.

because the material has only a very small hysteresis loop and corresponding a low remanent polarisation value. A curve of this approximation is displayed in Fig. 12 and the following empirically derived formula can be used to describe this shape:

$$D_0(E_{dc}) = 0.18 \cdot \frac{\exp(E_{dc}/E^*) - 1}{\exp(E_{dc}/E^*) + 1} \frac{\mathrm{As}}{\mathrm{m}^2} \quad \text{with} \quad E^* = 4\,\mathrm{MV/m} \tag{4}$$

In analogous form, the nearly quadratic bias field dependent strain $S_0(E_{dc})$ in parallel with the electric field is approximated by a non-linear but unambiguous curve. It is shown in Fig. 13 and can be described with Eq. (5):

$$S_0(E_{dc}) = 1.8 \cdot 10^{-3} \left\{ 1 - \exp\left[-\left(1.7 \cdot 10^{-7} \frac{\mathrm{m}}{\mathrm{V}} \cdot E_{dc} \right)^2 \right] \right\} \tag{5}$$

These last two equations are used in an iterative calculation cycle which is shown in Fig. 14 to estimate the electrical and mechanical operating point under an electric bias field. Firstly, the electric field distribution is calculated from a stress and polarisation free initial state with constant permittivities for the whole dielectric material and the applied electric bias voltage. In the second step the permittivity values are locally changed according to this field distribution, so that the electric displacement $D_0(E_{dc})$ [corresponding to Eq. (4)] will be adequately calculated in this region. In the next step the strain distribution, which is introduced by the locally varying electric field, is calculated with Eq. (5). As a first approach this is implemented in the model by using field dependent coefficients of thermal expansion and a constant temperature difference to the fixed reference temperature for the whole model. The iteration cycle is finished, when the permittivity change in each element of the model to the former calculated value is less than 1%. Otherwise, the new electric field distribution is calculated for the changed permittivity values and the last two steps are repeated. A feedback of the mechanical strain onto the electric field can be neglected.[4,5] The result is the electric field distribution and the mechanical strain in the large signal operating point due to an applied dc bias voltage. This is the starting point to apply local distributions of small signal material characteristics for bias field dependent permittivities and the piezoelectric coefficients. Details on this modelling can be found in Ref. 6. Small signal device simulations under electrical bias fields are published elsewhere.[7]

The mechanical behaviour of the dielectric was assumed to be linear elastic. A bilinear kinematic hardening law was used for the metal parts of the components. A detailed description of the temperature dependent material properties used in the simulation is given elsewhere.[8] The simulation of stresses due to the sintering of layered MLC structures is approached by the assumption of different material expansions of the dielectric and the inner electrodes. The difference in expansion was estimated from the material structure observed at a polished cross-section of a sintered MLC to be approximately 20%. This led to tensile peak-stresses near the end of the inner electrodes of the MLC whereas the outer surface of the MLC is mainly stressed by compression. As no fracture origin was related to the ends of the inner electrodes, it has been concluded that the estimated level of the tensile peak stresses is much too high. Therefore, only the global stress distribution (without the peak stresses) has been considered for Weibull analysis.

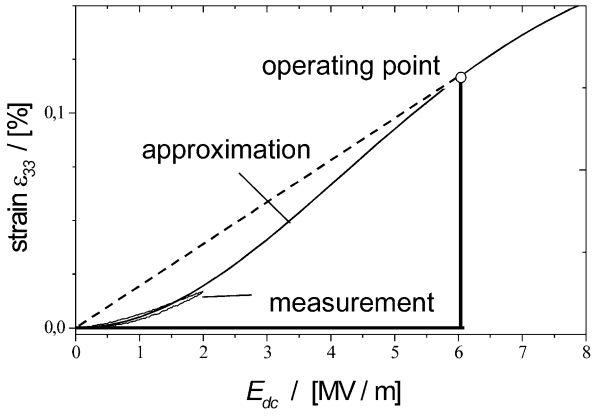

Fig. 13. Approximation curve for the bias field dependency of the mechanical strain S_{33} for the modelling of the large signal operating point.

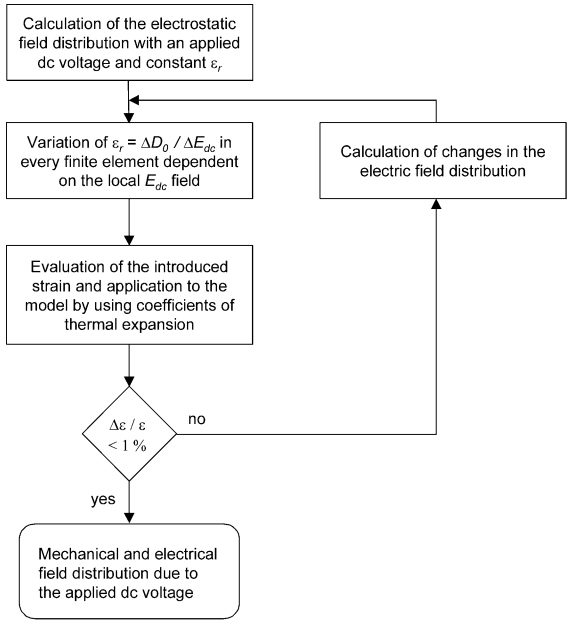

Fig. 14. Iteration cycle for the implementation of a large signal operating point for a structure with a local field distribution.

3.2. Design of the finite-element model

The two-dimensional model is created and calculated by the FEM software ANSYS®. It is programmed using the ANSYS® internal programming language APDL.[11] All values defining the geometry, the material properties, the process, and the loading conditions are parameter based and may be changed. A typical design of the model is given in Fig. 15, the FE-mesh is not shown. The geometry was taken from polished cross sections of soldered MLCs. The total inner and outer geometry including the inner electrodes, the layered design of the termination, the soft solder, and the printed circuit board is modelled. Just half of the cross-section of a MLC is modelled due to symmetry. The FE-mesh density is highest near the edge of the termination and at the end of the inner electrodes. A typical finite-element size in this region is about 1 μm. A more detailed description of the model and the temperature dependent material properties used is given elsewhere.[8,9] The model is suitable for the calculation of thermal, mechanical, and electrical load cases.

3.3. Calculation steps and evaluation

The calculations in this paper are divided in two principle parts which are the calculation of stresses and the evaluation of these stresses. The stress calculation itself is separated into three kinds of stresses which are the residual, joining and load stresses (Fig. 16). The load stresses are furthermore distinguished by their kind of loads which are bending and electrical loads. The superposition of all these stresses leads to the total stress distribution of MLCs as a function of their geometry, material properties, processing parameters, and loads. A total of more than 100 parameters are involved in the calculation. Nevertheless, this is just an approach and a lot of parameters are not exactly known or neglected at all. For example, the model is still two-dimensional even if there are some factors calculated by rough three-dimensional calculations to cover the influence of the component width.[6–10]

The total stress distribution can be evaluated to perform reliability analyses. The reliability is calculated by the two-parameter Weibull theory.[12,13] The failure probability F_V for volume flaws (index V) is given by

$$F_V = 1 - \mathrm{e}^{\left[-\frac{V_{eff}}{V_0}\left(\frac{\sigma_p}{\sigma_{OV}}\right)^{m_V}\right]}, \tag{6}$$

where

$$V_{eff} = \int_V \left(\frac{\sigma(x,\ y,\ z)}{\sigma_p}\right)^{m_V} dV \tag{7}$$

and $\sigma(x, y, z)$ denotes the tensile stress distribution, σ_p the predestined (or peak) stress, m_V the Weibull modulus

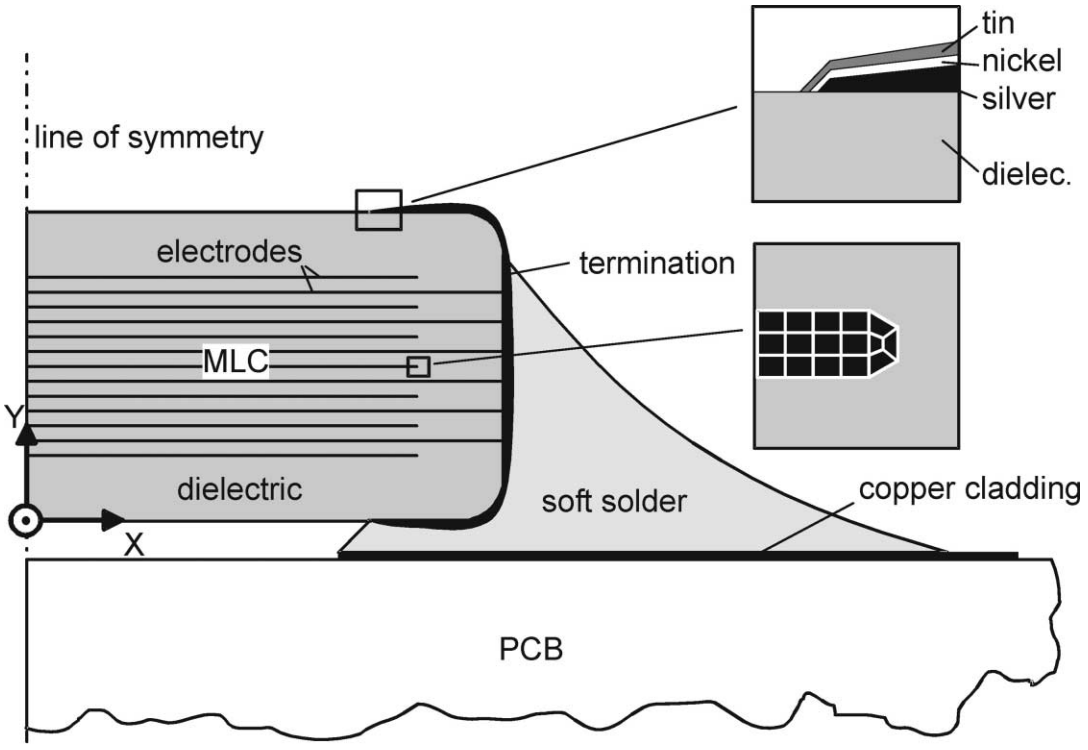

Fig. 15. Design of the FEM-model of a soldered MLC, mesh not shown.

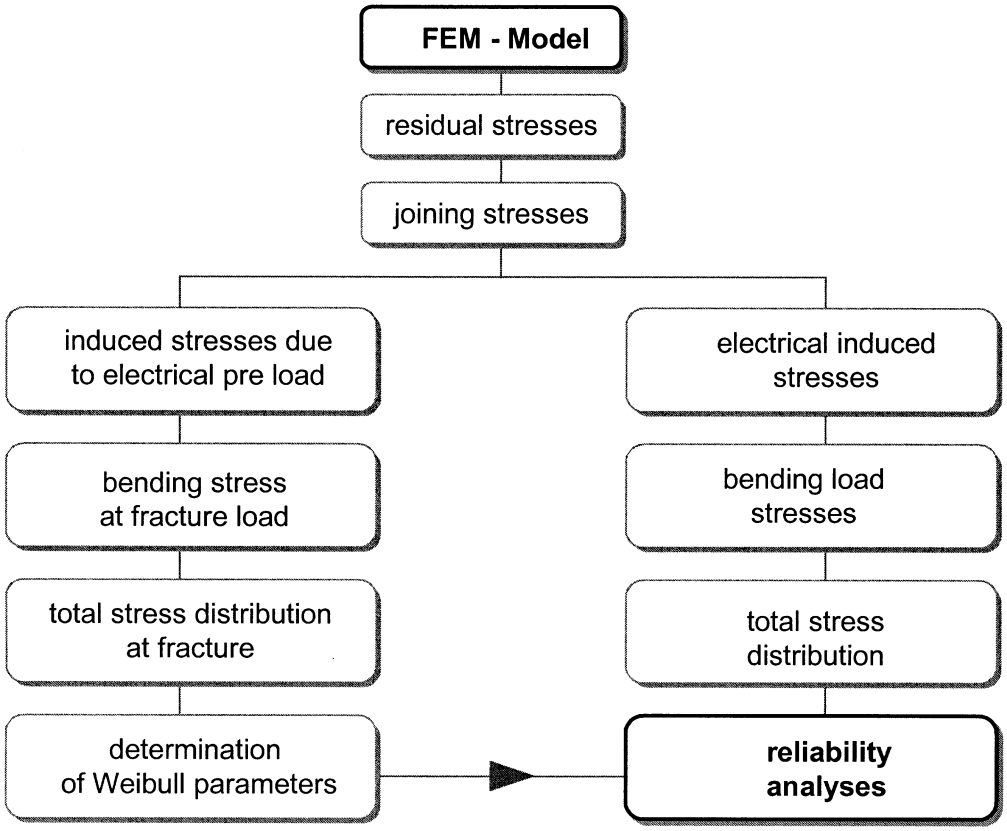

Fig. 16. Flow chart of FEM simulation.

for volume flaws, V_0 the unit volume (1 mm^3), V_{eff} the effective volume, and σ_{OV} the characteristic strength. A post processor routine was established which reads the FEM output and calculates the failure probability with special respect to changing stress fields in time.[8] If the stress calculation is done for the measured fracture loads, the fracture stresses can be calculated and lead to the mean Weibull parameters $\tilde{\sigma}_{OV}$ and $\tilde{m}_V$ for all measurement series. These parameters are then used to evaluate further stress calculations. As no universal multi-axial failure criterion exists, the principle of independent action (PIA) related to the principle tensile stresses has been applied.

4. Simulation results

4.1. Residual stresses

The residual stresses due to the manufacturing process of MLCs were calculated under the assumption of different thermal expansion of the dielectric and the inner electrodes as well as for different sintering shrinkage. These stresses were superimposed by the stresses caused by the application of the termination. The tumbling process, which is known to create stresses in the component surface,[14] is neglected. An offset of the calculated stresses compared with the measured stresses is therefore expected. A comparison between the calculated and the measured residual stress σ_x at the surface of a size 1210 MLC with 5 inner electrodes is shown in Fig. 17. The qualitatively course of the calculated residual stress matches well with the measured one except off an offset which may be explained by the tumbling process. The tensile stresses near the termination are calculated as a result of their firing on. The compressive stresses in the middle of the component are a result of the deformation of the MLC chip during sintering. The two calculated minima are affected by the interaction of the termination burn in

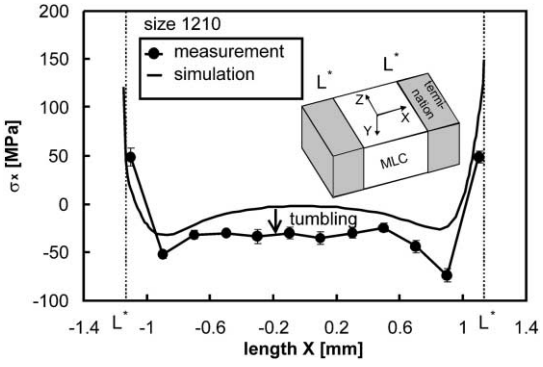

Fig. 17. Comparison of calculated and measured residual stress σ_x at the component surface.

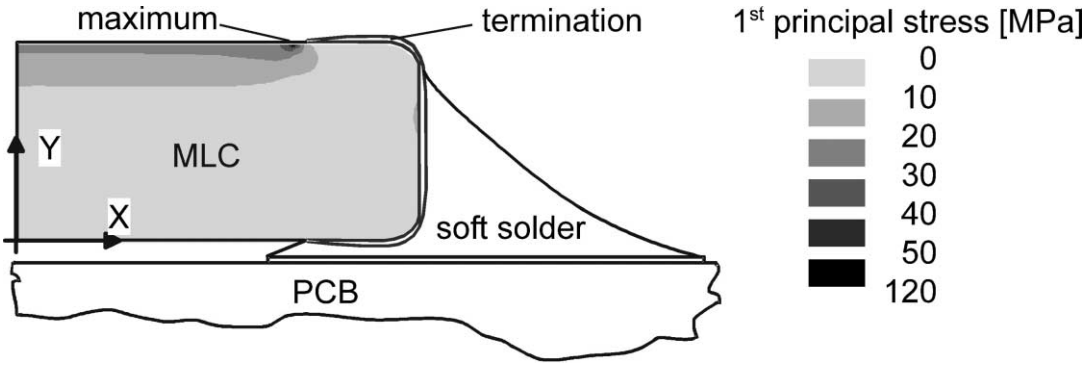

Fig. 18. Calculated joining stress of a soldered 1206 MLC (56 nF), soldering temperature $T_{sold} = 250$ °C, preheating temperature $T_{pre} = 250$ °C.

and the sintering deformation of the MLC chip near the end of the termination. An influence on the stress minima as a function of the termination size and the length of the inner electrodes (respectively the electrical inactive region under the termination) was found.

4.2. Joining stresses

The joining stresses are the stresses which remain in the MLC after soldering due to the different thermal expansions of the MLC, the solder, and the printed circuit board. The numerical model can be used to compute the transient temperature distribution during wave soldering and cooling as well as the concerning stress distribution. During cooling, the solder temperature is observed and the solder is turned solid when its temperature falls below the solidus temperature.[1] In this work the joining stresses are calculated for a preheated ($T_{pre} = 250$ °C) MLC and a soldering temperature of $T_{sold} = 250$ °C. The resulting stress distribution at the ambient temperature is shown in Fig. 18. The maximum tensile stress is calculated at the upper cover layer of the MLC near to the edge of the termination. The joining stresses superimpose the residual stresses and give the total stress distribution after soldering. Since high tensile residual stresses are also located near the termination edge (Fig. 17) the maximum total tensile stresses after soldering are calculated here. The asymmetric distribution of the residual stress in Fig. 17 is caused by the alternating links of the inner electrodes to the termination contacts. Fig. 19 shows the polished cross-section of a soldered MLC under the edge of the upper cover layer. A crack can be found starting near the edge of the silver layer where the maximum tensile stresses were calculated.

4.3. Load stresses

Beside the residual and joining (pre-)stresses, stresses due to electrical, mechanical, and/or thermal loads may cause failures of the device under operation. In principle, the numerical model is capable to calculate the mechanical stress field, the temperature distribution, and the electrical field as a reaction on electrical, thermal, and mechanical loading. In this paper the focus is set on mechanical and electrical loading. A bending test of soldered MLCs with and without electrical loading was simulated. The simulated test had the same geometry, load and boundary conditions as the performed four-point bending test described in Section 2.3. A calculated distribution of the first principal stress for a load moment of $M = 0.12$ Nm is shown in Fig. 20. Tensile stresses are located in the lower cover layer (PCB side) of the MLC. The stresses reach a maximum near the edge of the termination.

The electrical loading results in an inhomogeneous electric field and mechanical stress distribution evoked by the piezoelectric coupling. Fig. 21 shows the calculated electric field distribution in the model of the soldered MLC of type 1206 with 56 nF in the operating point at an electrical bias voltage of $U_{dc} = 50$ V. The material parameters have been adapted to the local field distribution according to the iteration cycle described in Section 3.1. The electric field is homogeneous in the region between the internal electrodes in the middle part of the MLC. The field is distorted and locally much higher at the ends of the internal electrodes which are

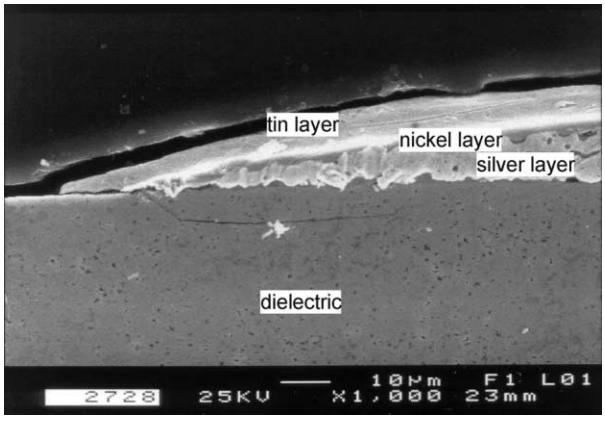

Fig. 19. Crack in the cover layer under the termination of a soldered ($T_{sold} = 250$ °C, $T_{pre} = 250$ °C) MLC.

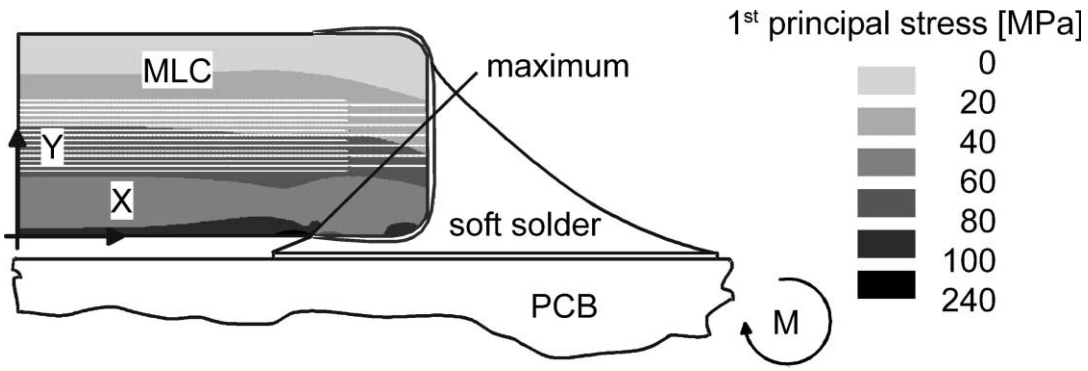

Fig. 20. Calculated bending stress of a 1206 MLC (56 nF), bending moment $M = 0.12$ Nm, PCB width $b = 1.6$ mm.

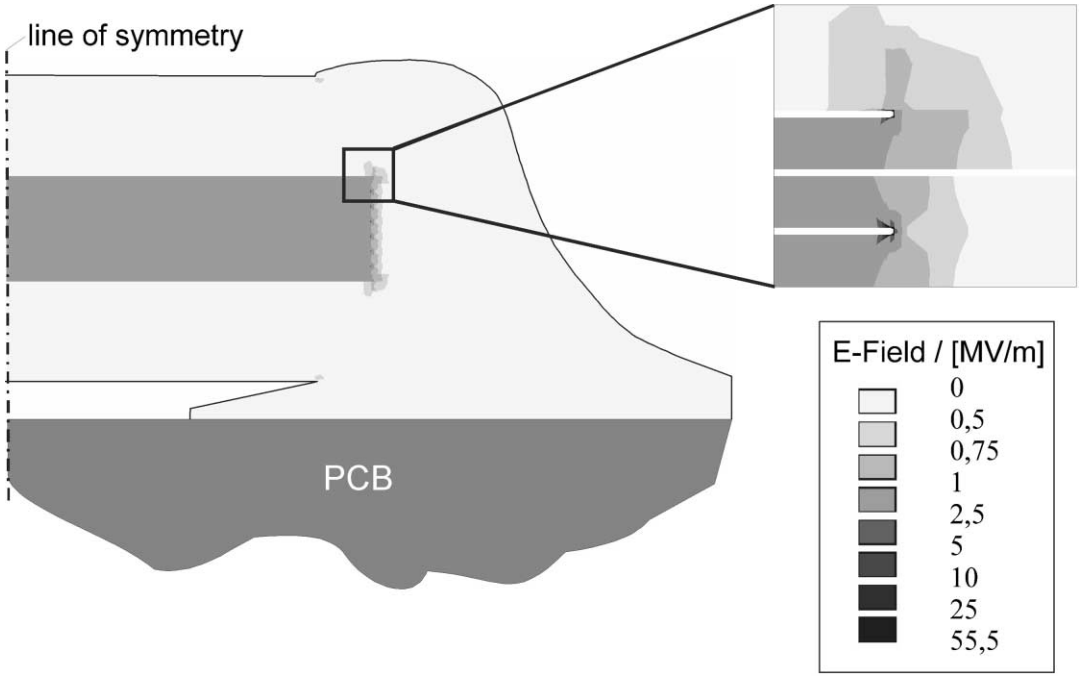

Fig. 21. Electric field distribution calculated with the 2D MLC model soldered on a printed circuit board for an operating point of $U_{dc} = 50$ V.

not connected to the modelled termination contact. This can be seen in the detailed view of this region in Fig. 21. This electric field distribution effects a mechanical stress distribution in the operating point which is displayed in Fig. 22. Homogeneous tensile stresses occur in parallel to the internal electrodes in the electrical active region in the middle of the MLC. Much higher stresses can be found at the ends of the internal electrodes where the electric field has its maximum too. Further details on this tensile stress distribution can be found in[15] and correspond well with possible crack propagations in multilayer actuators observed by Schneider et al.[16]

4.4. Reliability under total stress

The superposition of the residual, the joining, and the load stresses leads to the total stress distribution. Performing the calculation for the measured fracture loads (mechanical and electrical) gives the fracture stresses. Applying the theory of Weibull to these stresses results in the Weibull plot in Fig. 23. The failure probability F_V is plotted versus the fracture stresses, which are the peak stresses σ_p. The stress distribution during bending changes due to the plastic deformation of the soft solder. Therefore, the effective volume is not constant which is necessary for the Weibull plot. For this reason every measured fracture stress is iteratively calculated into a fracture stress for a constant effective volume of $V_{eff} = V_0 = 1$ mm^3. From all measurement series the mean Weibull parameters are derived to be $\tilde{\sigma}_{OV} = 96.7$ MPa and $\tilde{m}_V = 16.8$. The position of the single measurements in relation to the confidence interval for a confidence level of 95% indicates, that the assumption of one set of Weibull parameters valid for all measurement

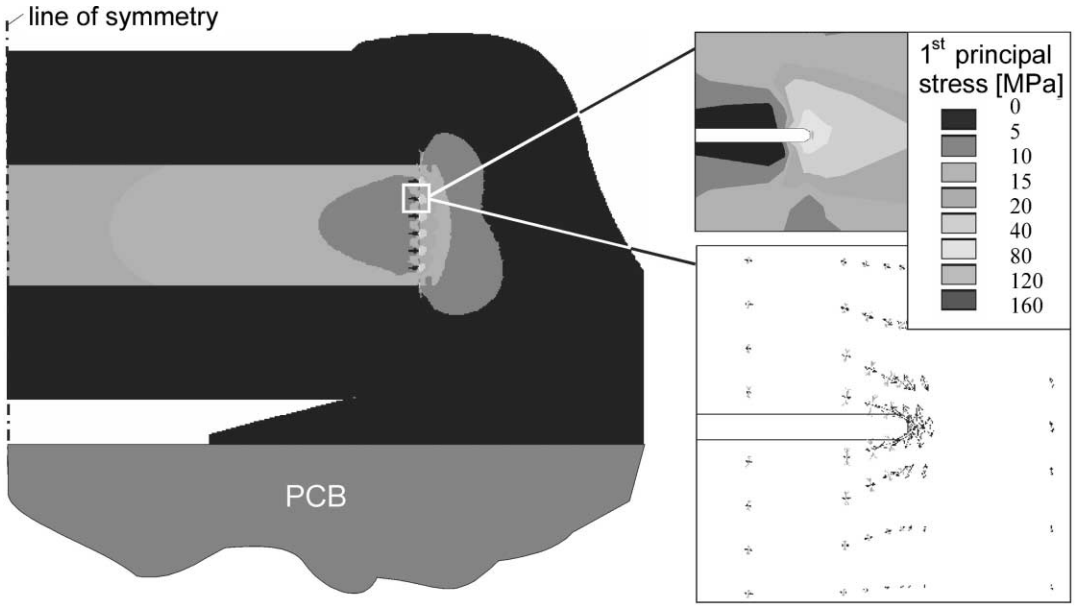

Fig. 22. First principal stress distribution in the soldered MLC due to the applied electric load of $U_{dc} = 50$ V.

series is not satisfied. Three reasons are under consideration:

1. There are dominant surface flaws or a combination of surface and volume flaws.
2. The stress distribution is calculated not exactly enough.
3. The components have different microstructures from type to type.

The results were evaluated once more under the assumption of critical surface flaws which leads to a different but not more precise distribution.[9] An improvement on the stress distribution is expected for a three-dimensional model instead of a two-dimensional and for a more detailed simulation of the residual stresses (tumbling).

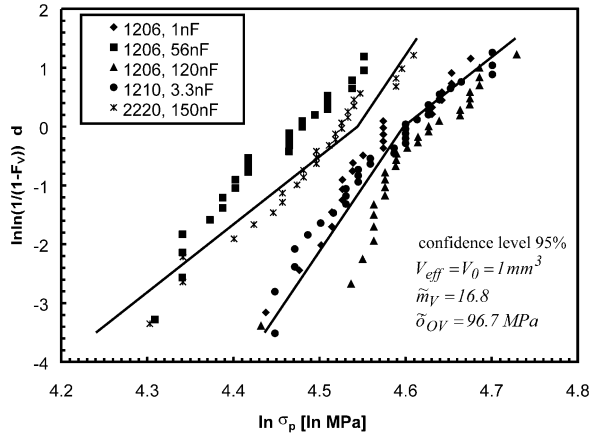

Fig. 23. Weibull plot and confidence interval of five soldered and bent MLC sizes.

The measured Weibull parameters show a high Weibull modulus m_V and a low characteristic strength σ_{OV} in comparison to the literature.[3,17,18] A possible explanation is that the soldered MLCs show a high local tensile stress concentration near the termination edges due to the firing on of the terminations. Under bending, additional tensile stresses with a peak near the lower termination superimpose on these residual stresses. This may result in a local critical stress near the termination edge during bending which leads to a local crack. This local crack relieves the elastic energy stored in the stress concentration without being critical for the remaining global stress. If the global stress reaches a critical value for the pre-cracked structure, the complete component fails. Evaluating a component with such a crack behaviour with the Weibull theory would give a high Weibull modulus and a low characteristic strength since there are always nearly the same crack sizes at the same position.

Two different sets of parameters seem to describe the measurements in Fig. 23 more precise. One set for the series of component type 1206 (56 nF) and type 2220 (150 nF), the other for the series of component type 1206 (1 and 120 nF) and type 1210 (3.3 nF). Since the following parameter studies are based on the type 1206 MLC with 56 nF, the mean Weibull parameters ($\tilde{\sigma}_{OV} = 88.5$ MPa, $\tilde{m}_V = 16.5$) of this series are used for the calculation of the failure probability. Fig. 24 shows the failure probability under bending load calculated for the variation of the solder fillet height. A lower height leads to higher failure probabilities. A strong influence on the failure probability under bending load was calculated for the overlapping length (termination width) of the terminations and the dielectric (not shown).

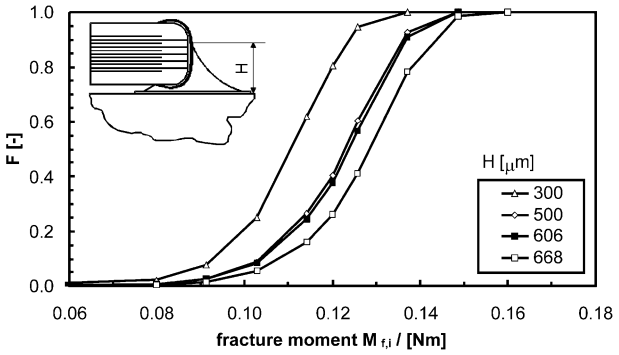

Fig. 24. Calculated failure probability of a soldered and bent 1206 MLC (56 nF) with variation of the solder fillet height H.

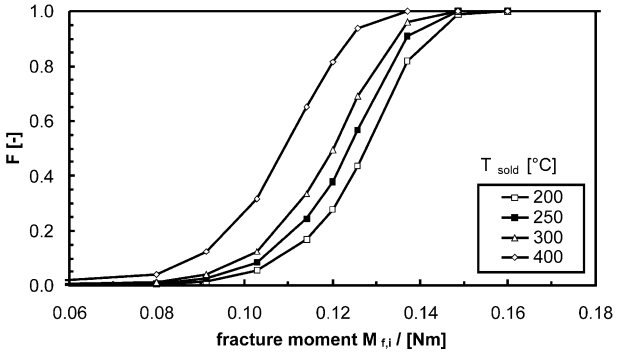

Fig. 25. Calculated failure probability of a soldered and bent 1206 MLC (56 nF) with variation of the soldering temperature.

Shorter terminations result in higher failure probabilities under bending load. Both effects can be found at real components.[19] Lower failure probabilities are calculated for higher numbers of inner electrodes as measured by Al-Saffar.[20] As an example for the variation of process parameters the impact of the soldering temperature on the failure probability under bending load is studied (Fig. 25). Higher soldering temperatures produce higher thermal expansions of the MLC compared to the PCB which leads to less compressive joining stresses in the lower cover layer at room temperature. Therefore, the failure probability under bending load rises with the soldering temperature.

5. Conclusions

This work presents an experimentally supported modelling of the coupled electrical–mechanical–thermal characteristics of ceramic multilayer capacitors. Objective of the work is the modelling of the non-linear coupled material characteristics for calculations of the integral device behaviour and the internal mechanical and electrical stress distributions. The results allow a description and possible improvement of the short-time reliability under particular load cases.

For an exact modelling of the device behaviour the electrical and piezoelectric large and small signal characteristics have been measured experimentally. Residual stress measurements have been performed at the surface of MLCs. These are used for comparison and verification with simulated residual stress data.

A two-dimensional parameter-based model has been developed for the simulations. This model includes the detailed internal and external structure of a MLC which is soldered on a PCB and can be easily adapted to different device geometry's. The capabilities of the program ANSYS® have been extended to include routines to apply non-linear electrical and piezoelectric material characteristics according to a large signal operation point depending on the local field distribution in the device. These routines are used to calculate the electric field distribution under an electrical bias voltage and the evoked mechanical stresses under this electrical loading.

To demonstrate the capabilities of the model and the coupled calculations typical four point bending tests with an additional electrical loading have been performed. The bending tests have been carried out with 5 lots of soldered MLCs of different size with and without an applied bias voltage. The following results have been obtained:

- The finite element models of the different MLCs have been used together with the measured fracture moments to calculate the mechanical stress distribution in the devices at the moment of fracture.
- Residual and joining stress distributions and stress distributions due to the electrical loading have been calculated too and superpositioned to the mechanical loading stress distributions. This total stress distribution is used to estimate the mechanical short-time reliability by the two-parameter Weibull theory.
- It can be shown that the electrical loading has no influence on the fracture probability of the soldered devices in the bending test because the electrical influenced stresses are located mainly in the regions of the internal electrodes whereas the cracks which lead to failure start at the lower end of the termination contacts.
- It is not possible to assume one set of Weibull parameter for the different MLC lots which fulfils a confidence level of 95%. The different series have to be described by at least two sets of Weibull parameters. Reasons for this behaviour could lie in different microstructures of the components, a combination of surface and volume flaws, or in an inaccuracy in the calculation of the stress distribution.
- The developed model has been used for variation calculations of geometrical and process parameters to estimate their impact on the failure probability.

Further improvements can be achieved with a more detailed simulation of the residual stresses and the transition to three-dimensional models. One important advantage of the model is the possibility to calculate the behaviour of MLCs made of other materials and material compositions. Furthermore, on the basis of the model character of the MLC structure, it is easy to apply the results to comparable multilayer devices.

Acknowledgements

The authors wish to thank the Deutsche Forschungsgemeinschaft (German Research Society) for financial support and Frank Schmitz (IKKM, RWTH Aachen) for the residual stress measurements and discussion.

References

1. Hennings, D. and Rosenstein, G., Temperature-stable dielectrics based on chemically inhomogeneous $BaTiO_3$. *J. Am. Ceram. Soc.*, 1984, **67**, 249–254.
2. Pertsch, P., Pan, M.-J., Vedula, V. R., Yoshikawa, S., Park, S.-E. and Shrout, T. R., Characteristics of electromechanical solid state multilayer actuators. In *Symposium on Applications of Ferroelectrics*. ISAF IX, 24–27 August 1999, Montreux.
3. Koripella, C. R., Mechanical behavior of ceramic capacitors. *IEEE Transactions on Components, Hybrids, and Manufacturing Technology*, 1991, **14**(4), 718–724.
4. Gong, X., Stresses near the end of an internal electrode in multilayer electrostrictive ceramic acutators. *Mater. Res. Soc. Symp. Proc.*, 1995, **360**, 83–88.
5. Hao, T. H., Gong, X. and Suo, Z., Fracture mechanics for the design of ceramic multilayer actuators. *J. Mech. Phys. Solids*, 1996, **44**, 23–48.
6. Prume, K., *Modellierung und Simulation der elektrisch-thermisch-mechanisch gekoppelten Eigenschaften keramischer Vielschichtkondensatoren*. D82 (Diss. RWTH Aachen), 2000.
7. Prume, K., Waser, R., Franken, K. and Maier, H. R., Finite-element analysis of ceramic multilayer capacitors: modelling and electrical impedance spectroscopy for a non-destructive failure test. *J. Am. Ceram. Soc.*, 2000, **83**(5), 1153–1159.
8. Franken, K., Maier, H. R., Prume, K. and Waser, R., Finite-element analysis of ceramic multilayer capacitors: failure probability caused by wave soldering and bending loads. *J. Am. Ceram. Soc.*, 2000, **83**(6), 1433–1440.
9. Franken, K., *Zuverlässigkeitsmodellierung von Vielschichtkondensatoren unter Eigen-, Verbund- und Lastspannungen*. D82 (Diss. RWTH Aachen), 2000.
10. Franken, K. and Maier, H. R., Weibull analysis of soldered MLC under bending load stress. *J. Eur. Ceram. Soc.*, 1999, **19**, 1307–1310.
11. SAS IP, Inc©. *Ansys User's Manual, Volume I—Procedures*, September 1994.
12. Weibull, W., The phenomenon of rupture in solids. In: *Ingeniörs Vetenskaps Akademien*, *Handlingar*, Stockholm, 1939, **153**.
13. Weibull, W., A statistical distribution function of wide applicability. *J. Appl. Mech., 1951, 9*.
14. de With, G. and Sweegers, N., The effect of erosional wear on strength and residual stress during shaping of ceramic multilayer capacitors. *Wear*, 1995, **188**, 142–149.
15. Prume, K., Franken, K., Waser, R. and Maier, H. R., 2D finite-element analysis of the coupled electrical–mechanical–thermal characteristics of ceramic multilayer capacitors. In: *Proc. Electroceramics V*, Aveiro, 1996,**1**, 255-258.
16. Schneider, G. A., Rostek, A., Zickgraf, B. and Aldinger, F., Crack growth in ferroelectric ceramics under mechanical and electrical loading. *Proc. Electroceramics IV, Aachen*, 1994, **2**, 1211–1216.
17. de With, G., Structural integrity of ceramic multilayer capacitor materials and ceramic multilayer capacitors. *J. Eur. Ceram. Soc.*, 1993, **12**, 323–336.
18. Bergenthal, J., Mechanical strength properties of multilayer ceramic chip capacitors. In: *11th Capacitor and Resistor Technology Symposium (CARTS)*, 1991, KEMET F-2106 6/91.
19. Bergenthal, J., Ceramic chip capacitors Flex Cracks—understanding and solutions. *Kemet Electronics Corporation*, Greenville, 1998.
20. Al-Saffar, R., Freer, R., Tribick, I. and Ward, P., Flexure strength of multilayer ceramic capacitors. *Br. Ceram. Trans.*, 1999, **98**(5), 241–245.